Absorption Cross Sections of Formaldehyde at Wavelengths from 300 to 340 nm at 294 and 245 K

Carina A. Smith, Francis D. Pope,[†] Bríd Cronin, Clare B. Parkes, and Andrew J. Orr-Ewing*

School of Chemistry, University of Bristol, Cantock's Close, Bristol BS8 1TS, U.K.

Received: June 14, 2006; In Final Form: August 29, 2006

Absorption cross sections for the $\tilde{A}_1A_2-\tilde{X}_1A_1$ electronic transition of formaldehyde have been measured by ultraviolet (UV) laser absorption spectroscopy in the tropospherically significant wavelength range 300−340 nm, over which HCHO is photochemically active. Absorption cross sections are reported at two temperatures, 294 and 245 K and at a spectral resolution of 0.0035 nm (0.35 cm^{-1}). At this resolution, greater peak absorption cross sections are obtained for many of the sharp spectral features than were previously reported. To simulate atmospheric conditions in the troposphere, the effects of adding a pressure of nitrogen of up to 500 Torr and of reduced sample temperature were investigated. The overall magnitudes of peak absorption cross sections are largely unaffected by the added pressure of nitrogen, but a modest degree of pressure broadening (0.2−0.3 cm^{-1} atm^{-1}) is evident in the line shapes. Computer simulations of spectra have been optimized by comparison with wavelength-dependent formaldehyde absorption cross sections for each major vibronic band in the chosen wavelength range. Experimental and computer simulated spectra at 294 and 245 K are compared to test the reliability of the computer simulations for quantification of the effects of temperature on absorption cross sections. All experimental absorption cross section data and tables of input parameters for spectral simulations are available as Supporting Information.

1. Introduction

Formaldehyde (HCHO) is a naturally occurring atmospheric compound with an active and important role in the photochemistry of the troposphere. It is formed as an intermediate in the oxidation pathways of many biogenic and anthropogenic volatile organic compounds (VOCs) and is a source of HO_x (OH and HO_2), thus playing an important part in the interrelated chemistries of ozone and the HO_x and NO_x (NO and NO_2) cycles. A global tropospheric background of HCHO is present as a result of oxidation of methane (which has a tropospheric average mixing ratio of ∼1.72 parts per million by volume (ppmv)),[1] and other non-methane VOCs including isoprene, the dominant hydrocarbon released by many plant species.[2] Anthropogenic sources of HCHO include vehicular and industrial emissions. Measured concentrations of HCHO range from ∼50 pptv (parts per trillion by volume) in clean Antarctic tropospheric air in winter,[3] to 15−20 ppbv (parts per billion by volume) in the London urban area,[4] and ≤70 ppbv in the Los Angeles area.[5] There are two major loss pathways for HCHO, photolysis and reaction with the hydroxyl radical (OH), which account for the atmospheric lifetime of HCHO being on the order of a few hours.[6]

The HO_x family is central to the photochemistry of the troposphere, and its primary source is the reaction of O(^{1}D) atoms, formed from ozone photolysis, with water vapor. Water concentrations in the upper troposphere are low, however, and HO_x production via this route is thus expected to be small in magnitude. Predictions from models containing only ozone, water, and methane chemistry,[7] however, underestimate HO_x concentrations both in the upper troposphere and in the boundary layer.[8,9] Photolysis of formaldehyde and subsequent reaction of the radical products, H and HCO, with oxygen is an important additional source of HO_x which must be correctly incorporated into current models of the chemistry of these regions.

Absorption of ultraviolet (UV) radiation by formaldehyde in the wavelength range 260−360 nm occurs via an electronic transition from the ground state to the first excited singlet state, $S_1 \leftarrow S_0$, giving rise to the $\tilde{A}^1A_2-\tilde{X}^1A_1$ band system, which consists of an extended progression of vibronic bands. As a consequence of electric dipole selection rules, this electronic transition is symmetry forbidden but can become allowed through vibronic coupling; hence the $\tilde{A}-\tilde{X}$ band of formaldehyde has relatively small absorption cross sections for an electronic transition. In addition to possible quenching and radiative decay of the excited state, there are two competing dissociative channels following absorption, leading either to molecular or radical products:

$$\mathrm{HCHO} + h\nu \rightarrow \mathrm{H_2} + \mathrm{CO} \qquad (\lambda < 360\ \mathrm{nm}) \qquad (1)$$

$$\mathrm{HCHO} + h\nu \rightarrow \mathrm{H} + \mathrm{HCO} \qquad (\lambda < 330\ \mathrm{nm}) \qquad (2)$$

The wavelengths in brackets are derived from threshold energies for the opening of each dissociation channel.[10] There is an additional decay channel occurring at wavelengths below 283 nm, forming radical products H + H + CO, but it is not important in the troposphere. In the case of channel 1, the threshold energy corresponds to the barrier height on the S_0 state potential energy surface (PES), and for channel 2, it is the asymptotic energy for C−H bond breaking via the S_0 PES. Both photolysis channels have significant atmospheric consequences: channel 1 is a source of CO, and the reaction of the atomic and radical products from channel 2 with O_2 produces

---

* Author for correspondence. E-mail: a.orr-ewing@bris.ac.uk. Fax: +44 117 925 0612. Tel: +44 117 928 7672.

[†] Current address: Jet Propulsion Laboratory, M/S 183-901, 4800 Oak Grove Drive, Pasadena, CA 91109.

10.1021/jp063713y CCC: $33.50

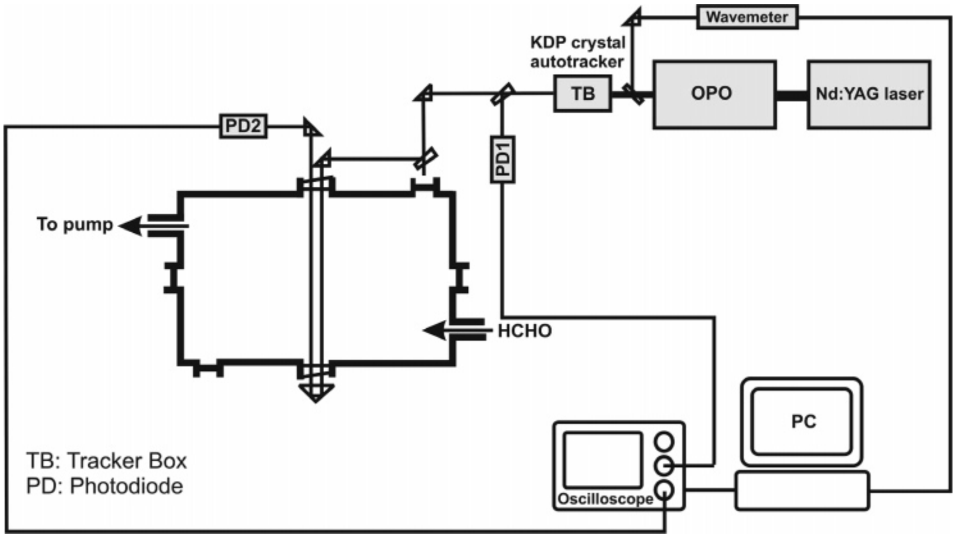

Figure 1. Schematic diagram of the experimental apparatus.

HO_2 radicals

$$H + O_2 + M \rightarrow HO_2 + M \qquad (3)$$

$$HCO + O_2 \rightarrow HO_2 + CO \qquad (4)$$

(which rapidly interconvert with OH, the major atmospheric oxidant). There are two important elements to the experimental characterization of HCHO photochemistry in the troposphere. The first is measurement of accurate absorption cross sections (the subject of this paper) and the second is determination of quantum yields for channel 2. These measurements are needed at high wavelength resolution to capture the consequences of the fine rovibronic structure in the HCHO $S_1 \leftarrow S_0$ absorption spectrum. Precise absorption cross sections as a function of UV wavelength are also necessary for interpretation of atmospheric retrievals of HCHO made using spectroscopic methods, whether, for example, by ground-based DOAS or by satellite spectrometers.[11−14]

Dieke and Kistiakowsky were the first to study the extensive progression of bands in the $\tilde{A}^1A_2-\tilde{X}^1A_1$ electronic absorption spectrum of HCHO,[15] which is the simplest carbonyl-containing molecule and exhibits resolved rotational features in its UV absorption spectrum. The first measurements of formaldehyde absorption cross sections in the UV region were made by McQuigg and Calvert in 1969.[16] Since then, several groups have measured these absorption cross sections including Bass et al.,[17] Cantrell et al.,[18] Rogers,[19] and Meller and Moortgat,[20] but at resolutions at or in excess of 1 cm^{-1} (0.01 nm at 320 nm) that were limited by the instruments employed. The spectrometer resolving powers were not sufficient to observe much of the rotational fine structure present in the absorption spectrum of the HCHO molecule. High resolution (0.027 cm^{-1}) Fourier transform UV spectra and HCHO absorption cross sections were reported by Co et al.[21] but spanned only the long wavelength absorption region from 351−356 nm. The current study employs UV laser absorption spectroscopy methods to measure HCHO absorption cross sections from 300 to 340 nm at superior resolution to any of the preceding measurements over this region. The measurements resolve additional sharply structured rotational features in the vibronic absorption bands; in the limit of Doppler broadening, the full widths at half-maximum height (fwhm) of lines corresponding to transitions between individual rovibrational levels would be 0.07 cm^{-1} (7×10^{-4} nm at $\lambda = 320$ nm) at $T = 294$ K. Ambient pressure and short (subnanosecond) excited-state lifetimes might serve to broaden the lines further.

Measuring HCHO absorption cross sections at a resolution higher than 1 cm^{-1} increases the likelihood of finding suitable absorption lines for atmospheric monitoring in a spectral window that is free from other absorbers. The higher resolution data are also essential to quantify precisely the impact of HCHO photochemistry on atmospheric HO_x and are thus part of a study currently underway in our laboratory to measure quantum yields of the radical products following HCHO photolysis, under atmospherically relevant conditions.[22] We report here absorption cross sections obtained at an instrument resolution estimated to be 0.35 cm^{-1}, measured by absorption of a UV laser beam tuned over the wavelength range 300−340 nm, and under conditions of low partial pressure of HCHO (∼1 Torr). The effects of reduced temperature and N_2 induced pressure broadening are also quantified over the same wavelength range. Preliminary measurements for the wavelength range 313−320 nm were reported previously but are greatly extended here.[23] Spectral simulations of the main vibronic bands of the $\tilde{A}^1A_2-\tilde{X}^1A_1$ electronic transition of HCHO at the two experimental temperatures are also described and provide a means of calculating absorption cross sections at temperatures other than 294 and 245 K.

2. Experimental Methods

The experimental setup has been described in detail previously and key features are summarized here.[22,23] The apparatus is shown in Figure 1. A custom-designed spectrometer was used to measure HCHO absorption cross sections and consisted of a tunable UV laser source and a chamber evacuated by turbomolecular and rotary vacuum pumps. The 600 × 200 × 300 mm rectangular vacuum chamber (which is also equipped with cavity ring-down spectroscopy facilities for HCO quantum yield measurements) was fitted with thermocouple temperature sensors and pressure gauges.

Tunable UV laser light was generated from either the frequency doubled output of a dye laser (Sirah Cobra Stretch) pumped by the 532 nm second harmonic of a Nd:YAG laser (Continuum Surelite III), or a Nd:YAG pumped optical parametric oscillator (OPO) (Spectra Physics MOPO 730-10). The manufacture-specified line widths of the fundamental visible beams from the dye laser and OPO are 0.0018 nm (0.044 cm^{-1} at 640 nm) and 0.13−0.19 cm^{-1} (depending on wavelength), respectively. Frequency doubling was achieved using a KDP crystal that was angle-tuned to maintain efficient UV generation using an auto tracker and UV energies in each ∼10 ns duration laser pulse were typically 1−1.5 mJ. A ≤10% fraction of the UV laser beam was separated from the main beam using a wedged beam splitter and entered and exited the vacuum chamber midway along, and perpendicular to, its long axis via wedged quartz windows mounted on opposite sides to form the double-pass absorption spectroscopy arrangement shown in Figure 1. The internal path length of the laser beam was 66.5 cm. The 0.5° wedges on the windows ensured that there were no fringe patterns arising from interference effects underlying the absorption spectra. Independent fast photodiodes, operated in photovoltaic mode, were used to measure the intensity of UV laser light entering and exiting the vacuum chamber, enabling quantification of both fluctuations in the laser power and the change in intensity resulting from passage through the spectrometer. This latter intensity change is a consequence of absorption by HCHO gas, scattering losses from the vacuum cell windows, and Rayleigh scattering from added pressures of nitrogen bath gas. All wavelength scans were repeated in the absence of HCHO but under otherwise identical experimental conditions to distinguish absorption losses from those caused by scattering and absorption. Quartz wedges (2°) were used to split a fraction (∼5%) of the UV beam into each photodiode without introducing fringing from interference effects as the laser wavelength was scanned. Quartz diffusers were placed in front of the photodiodes to average out the effects of any spatial structure in the UV laser beam and to ensure a linear response of the output signals to changes in the laser intensity. A wavemeter (Coherent Wavemaster) and an Etalon (with free spectral range of 2.05 cm^{-1} and transmission fringes monitored by a further photodiode) were used for wavelength calibration of the dye laser or OPO fundamental output. The wavemeter itself was calibrated by comparing to a simultaneously recorded laser induced fluorescence (LIF) spectrum of I_2 vapor. The majority of absorption measurements were undertaken using ≤10 μJ of UV energy per laser pulse (with pulse duration ∼8 ns), but to check for possible power broadening of lines (vide infra), restricted regions of the absorption spectrum were also scanned with pulse energies of 0.25 μJ (obtained by replacing a prism with a quartz-wedge beam splitter). The UV pulse energies were measured using a calibrated power meter.

HCHO was prepared according to the procedure of Spence and Wild:[24] paraformaldehyde (Aldrich prills, 95%) was heated to temperatures above 383 K to generate gaseous monomeric HCHO. The resultant gas was collected in a liquid nitrogen trap. Purification was achieved by passing the gas through a dry ice/acetone trap (195 K) to remove thermal decomposition impurities with vapor pressures lower than that for HCHO such as acetone and acetaldehyde, and then trap-to-trap distillation was performed with liquid nitrogen to remove any residual O_2 or N_2. HCHO was admitted to the main vacuum chamber via PTFE tubing by warming of the cryogenically trapped sample. Calibrated capacitance manometer gauges (0−10 and 0−1000 Torr, Edwards Barocel pressure sensors) were used to measure the pressure of HCHO gas and added nitrogen bath gas. Reduced temperatures in the chamber were achieved by passing cooled fluid (a mixture of triethoxyalkylsilanes) from a thermostat (Huber Unistat 360) through internal loops of copper piping. Two type-K thermocouples (placed at separate points along the laser beam axis to check there were no temperature gradients) were used to measure the temperature inside the chamber. The signals from the photodiodes monitoring the laser intensity at various points in the apparatus were digitized using an oscilloscope (LeCroy 6030) and transferred to a PC running LabView software via a GPIB interface for data accumulation and analysis. The wavemeter was connected directly to the computer via an RS232 serial port.

3. Results and Discussion

Analysis of incident and transmitted laser intensities was carried out using the Beer−Lambert law to determine formaldehyde absorption cross sections, σ, at each wavelength of the UV laser:

$$I = I_0 \exp(-\sigma l[\mathrm{HCHO}]) \tag{5}$$

In eq 5, I and I_0 are, respectively, the normalized intensities (as explained below) measured by a photodiode (PD2) located after the exit window, with and without HCHO present. [HCHO] is the known number density of HCHO, and l is the path length of 66.5 cm through the sample. Another photodiode (PD1) was located before the vacuum chamber to monitor the intensity of every laser pulse. Each signal recorded by PD2 was first normalized for fluctuating laser power by division by the equivalent signal from PD1. Scattering processes (such as Rayleigh scatter in the presence of nitrogen bath gas) and additional losses caused by the chamber windows cancel when taking the ratio of the two intensities in eq 5.

The use of the Beer−Lambert law is only valid to evaluate absorption cross sections if the absorbance is a linear function of the column density (the product of HCHO number density and optical path length). Of the previous literature studies of σ_{HCHO}, Bass et al.[17] and Rogers[19] neglected to take into account the nonlinearity in the absorbance of HCHO as a function of HCHO concentration that has been reported by other authors (Cantrell et al.;[18] Meller and Moortgat[20]). Cantrell et al.[18] noticed that deviations from the Beer−Lambert law typically occurred at the peak intensities of vibronic bands, and to account for the nonlinearity, cross sections extrapolated to values at zero number density were reported. In the current study, wavelength-dependent absorption cross sections for strong spectral features from a sample containing 1 Torr partial pressure of HCHO were compared with those obtained by extrapolating to zero pressure the cross sections measured at a range of HCHO partial pressures from 0.5 to 4 Torr. The extrapolated and 1 Torr spectrum cross sections were found to be in quantitative agreement (to much better than the uncertainties in cross section values specified later), thus validating the use of the Beer−Lambert law for data analysis under conditions of 1 Torr vapor pressure of HCHO. Cross sections measured at 2 and 4 Torr were, however, found to be lower than those from extrapolation to zero Torr. The use of a static sample of gaseous HCHO, at fixed partial pressure in the absorption chamber, was tested and justified by noting that measured absorption intensities remained unchanged for 1 h periods. Hence, the effects of wall losses and photodegradation and repolymerization of HCHO gas under low UV laser power conditions were negligible over the timescales of individual spectral scans. Spectra were typically accumulated over 0.7 nm wavelength intervals, with an overlap of adjacent spectra of 0.1 nm.

The line widths of the fundamental visible beams from the dye laser and OPO were determined by comparing experimentally measured low-pressure molecular iodine LIF spectra to computer simulations. The expected optimum UV bandwidths,

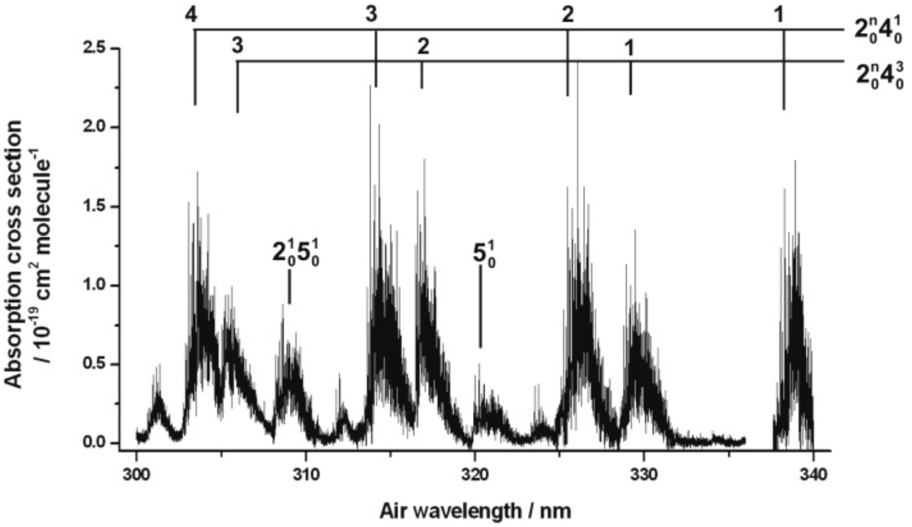

Figure 2. Absorption spectrum of the $\tilde{A}^1A_2-\tilde{X}^1A_1$ band system of HCHO recorded at the estimated Gaussian wavenumber resolution of 0.35 cm^{-1} (0.0035 nm) in the wavelength region 300−340 nm.

estimated as $\sqrt{2}$ times the measured line widths of the fundamental beams, were thus determined to be 0.17 and ≤0.20 cm^{-1} for the dye laser and OPO systems, respectively. Most of the absorption spectra were obtained using the OPO because of its wide wavelength tunbility. Spectral simulations of the absorption bands (see later), however, required incorporation of a line shape function with greater width to match the experimentally observed spectral lines. Two different line shape functions successfully reproduced experimental band contours and the intensities of resolved rotational structure when incorporated into spectral simulations. The first of these, as used previously by Pope et al.[23] is a Lorentzian function with fwhm of 0.45 cm^{-1}. The second line shape was constructed by addition of two Gaussian functions of equal areas, centered at the same point, but with fwhm values of 0.3 and 2 cm^{-1}. This latter, composite function closely resembles the Lorentzian line shape, with the broader of the two Gaussians providing the extra width in the profile wings that is characteristic of a Lorenztian line shape.

The line broadening over and above the expected contribution from the laser bandwidth was previously attributed to lifetime broadening of the predissociated rovibrational levels of the $\tilde{A}$ state. Lifetimes of these levels of ≤11 ps are required to account for ≥0.45 cm^{-1} of line broadening and are not consistent with previous reports of fluorescence lifetimes of a few ns or longer.[25] The experimentally observed line widths might, therefore, be a consequence of the true bandwidth of the UV from the frequency doubled OPO output, or broadening induced by the power of the UV laser pulses. The latter effect is a particular concern because of the possibility of optical pumping from the rovibrational levels of the $\tilde{A}$ state into the diffuse levels of the $\tilde{B}^1A''$-($^1B_2$) state via an electric-dipole allowed transition. This excitation is resonant at the wavelengths of the UV light and will shorten the lifetimes of levels of the $\tilde{A}$ state, resulting in spectral broadening. This possible broadening mechanism can be discounted, however, because spectra obtained with 0.25 and 10 μJ per pulse of UV energy were identical in their spectral resolution. We thus conclude that the frequency doubling of the OPO fundamental visible output generates UV radiation with a larger than optimum expected bandwidth of 0.3 cm^{-1}. The pedestal in the UV bandwidth function, described by the second, broader Gaussian contribution, may result from UV generation from additional frequency components underlying the narrow bandwidth part of the fundamental OPO output. HCHO absorption cross sections for the $2^3_0 4^1_0$ and $2^2_0 4^3_0$ bands (where M^a_b denotes a vibronic transition with *a* quanta of vibration in the upper ($\tilde{A}^1A_2$) state and *b* quanta in the lower ($\tilde{X}^1A_1$) state, and *M* defines the vibrational mode) were also recorded using the dye laser system, with frequency doubling of the output beam using the same KDP crystal; spectral resolutions and absorption cross sections were essentially identical for this and the OPO UV source.

In all the spectral simulations reported hereafter, the line shape functions used are a convolution of a 0.45 cm^{-1} (or wider, where specified) fwhm Lorentzian function and a 0.2 cm^{-1} fwhm Gaussian function. The resultant Voigt profile was chosen beause it is conveniently generated in the spectral simulation program and gives very satisfactory reproduction of experimentally observed band intensity contours and the shapes of sharp spectral lines.

3.1. Absorption Cross Sections at 294 K. Figure 2 shows the composite room temperature (294 K) absorption spectrum of HCHO arising from the $\tilde{A}^1A_2-\tilde{X}^1A_1$ excitation in the wavelength range 300−340 nm (33 320−29 400 cm^{-1}) obtained in the current study, plotted as absolute absorption cross sections against air wavelength. There is a small gap in the spectrum from 336−338 nm that was not scanned because of the weak absorption in this region. The spectrum is dominated by progressions in the C−O stretching vibration, ν_2, with the most prominent progressions coming from a series of b-type rovibrational bands, labeled as $2^n_0 4^1_0$ and $2^n_0 4^3_0$. The ν_4 mode, which is simultaneously excited, corresponds to the out-of-plane bend. The data plotted in Figure 2 are available in tabular form as Supporting Information.

There are several potential sources of uncertainty in the determinations of the absorption cross sections, including the precision of the calibrated pressure gauge (specified as 0.15% and therefore negligible), the uncertainty in the absorption path length (also negligible), the purity of the HCHO sample, the effects of non-Beer−Lambert absorption behavior (see above), and the stability of the UV laser intensity. To test the purity of the HCHO, infrared absorption spectra were taken and showed no evidence of bands other than those of HCHO. Uncertainties in absorption cross sections were therefore quantified by comparing the results of between 3 and 5 separate measurements of spectra for each vibronic band. Values plotted in the figures and listed in the supplementary data are the average of these

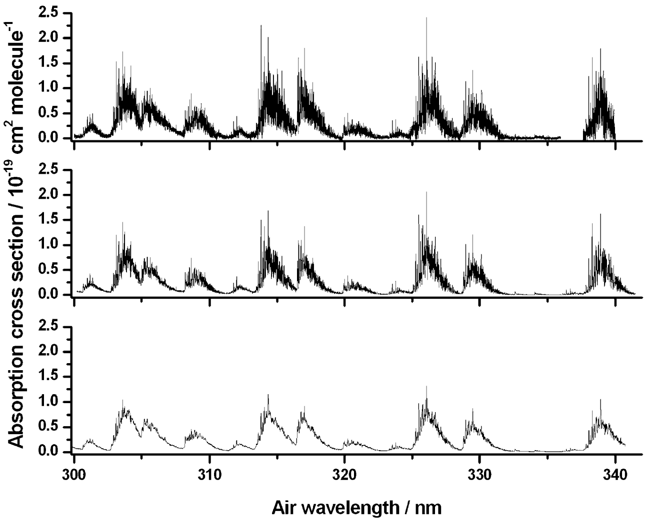

Figure 3. Comparison of the HCHO absorption cross sections obtained at a resolution of 0.35 cm^{-1} (this study, top panel) with two previous studies. Spectra were measured using a FT spectrometer with resolution of 1.00 cm^{-1} (0.011 nm at 330 nm) (middle panel, Cantrell et al.)[18] and using a diode array spectrometer with stated resolution of 0.028 nm at 320 nm (bottom panel, Meller and Moortgat).[20]

data sets. Rather than analyze variations at all wavelengths in the spectra, we selected representative lines of intermediate strength (peak absorption cross sections from 0.6 × 10^{-19} to 1.3 × 10^{-19} cm^2 molecule^{-1}) and determined the standard deviations of the cross sections at several points across the central part of each spectral feature. Uncertainties (1σ, expressed as percentages of the peak absorption cross sections of the chosen lines, evaluated as the average for three lines per vibrational band) were 9% ($2_0^4 4_0^1$), 10% ($2_0^3 4_0^3$), 5% ($2_0^1 5_0^1$), 4% ($2_0^3 4_0^1$), 8% ($2_0^2 4_0^3$), 9% ($2_0^2 4_0^1$), 6% ($2_0^1 4_0^3$), and 10% ($2_0^1 4_0^1$), with the larger values arising for wavelength regions where the UV laser operated less stably. If, as the above analysis suggests, the major source of uncertainty is fluctuations in the laser intensity, in combination with weak absorptions under our experimental conditions, with no significant sources of systematic error, rebinning or convolution of the spectral data into reduced resolution intervals will serve to reduce the uncertainties because of the effects of additional averaging. This suggestion is supported by the smaller (0.5−4%) uncertainties in the integrated band intensities presented in the following section. Although use of higher partial pressures of HCHO would improve the signal-to-noise ratios in our data, the derived absorption cross sections would be less reliable because of systematic errors introduced by deviations from Beer−Lambert law behavior.

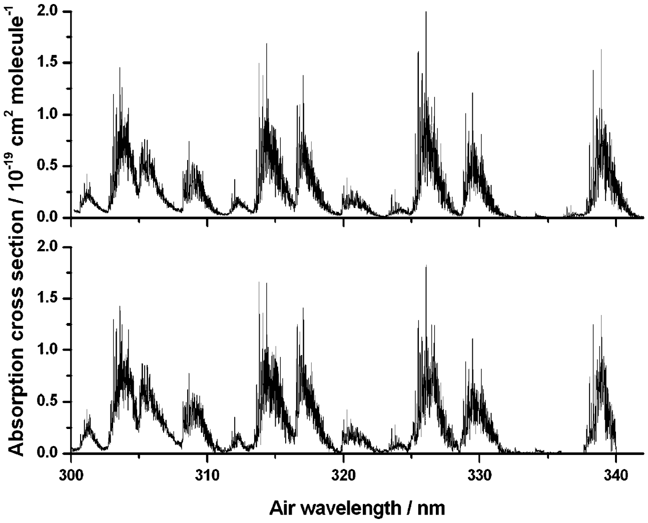

Figure 4. Comparison of the data of Cantrell et al.[18] with the current results processed to reduce the spectral resolution. Top panel: spectrum of Cantrell et al. measured at a resolution of 1.0 cm^{-1}. Bottom panel: data from the current study convoluted with a 1.0 cm^{-1} fwhm Gaussian function.

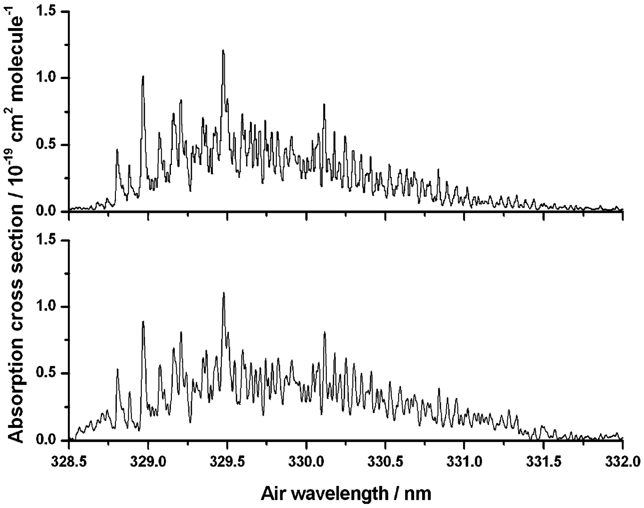

Figure 5. Expanded view of the spectra displayed in Figure 4 encompassing the $2_0^1 4_0^3$ vibronic band. Top panel: spectrum of Cantrell et al.[18] measured at a resolution of 1.0 cm^{-1}. Bottom panel: data from the current study convoluted with a 1.0 cm^{-1} fwhm Gaussian function.

3.2. Comparison with Previous Measurements. The current experimental data, measured at an estimated resolution of 0.35 cm^{-1} (0.0035 nm) with the dual Gaussian line shape function described earlier, are compared in Figure 3 with the results of the two previously published highest resolution studies, Cantrell et al.[18] and Meller and Moortgat.[20] The stated resolutions of the two preceding studies were 1.00 and 2.73 cm^{-1} (0.028 nm at wavelengths around 320 nm), respectively, although our best simulations of the data of Cantrell et al. require a Gaussian line shape of 1.4 cm^{-1}; simulations performed with a 1 cm^{-1} fwhm Gaussian function must be further convoluted with a Lorentzian function of fwhm 0.45 cm^{-1} for a satisfactory match to the experimental data. As is evident from Figure 3, peak HCHO absorption cross sections become higher as the resolution of the spectrometer approaches the widths of the sharpest spectral features. The current measurements provide a more complete (but still instrument limited) resolution of the highly structured bands that make up the HCHO $\tilde{A}-\tilde{X}$ absorption spectrum.

A quantitative comparison with previous measurements of $\sigma_{HCHO}(\lambda)$ was made by convoluting the current, higher resolution measurements with an instrument function chosen to mimic that of the spectrometer employed by Cantrell et al.[18] For lack of more precise information, the instrument function was taken to be Gaussian in form, with a fwhm set to the stated value of 1.00 cm^{-1}. Figure 4 shows a comparison of the convoluted spectrum with the data of Cantrell et al.[18] across the whole wavelength region measured in the current work, and an expanded region of the $2_0^1 4_0^3$ band is shown in Figure 5 to demonstrate clearly the level of agreement. The data from the current study have also been convoluted to mimic the instrument function of the spectrometer used by Meller and Moortgat,[20] and results are shown in the Supporting Information. Integrated absorption cross sections for each band, shown in Table 1, also

TABLE 1: 294 K Integrated Band Intensities for the Main Vibronic Bands in the 300−340 nm Region of the $\tilde{A}^1A_2-\tilde{X}^1A_1$ Electronic Absorption Spectrum of HCHO Compared with Results from Cantrell et al.[18] and Meller and Moortgat[20]

wavenumber interval/ cm^{-1}	vibrational band	integrated band intensity/ 10^{-17} cm^2 molecule^{-1} cm^{-1} Cantrell et al.	Meller and Moortgat	current study
32781−33023	$2^4_0 4^1_0$	1.227[a]	1.308	1.359 ± 0.022
32450−32781	$2^3_0 4^3_0$	0.918[a]	1.000	1.140 ± 0.028
32123−32450	$2^1_0 5^1_0$	0.649	0.655	0.724 ± 0.004
31600−31900	$2^3_0 4^1_0$	1.324	1.371	1.396 ± 0.010
31275−31600	$2^2_0 4^3_0$	0.976	1.022	1.122 ± 0.053
30425−30750	$2^2_0 4^1_0$	1.291	1.278	1.285 ± 0.010
30050−30425	$2^1_0 4^3_0$	0.791	0.804	0.842 ± 0.006
29403−29611	$2^1_0 4^1_0$	0.821[a]	0.803	0.756 ± 0.094

[a] Integrated band intensities for the results of Cantrell et al.[18] for a waveumber interval defined by the current study.

highlight the correspondence between the three data sets. Numerical integrations were performed using the Trapezium rule over the same wavenumber intervals as quoted by Cantrell et al.,[18] unless otherwise stated, and specified uncertainties in our values are one standard deviation from analysis of three separate measurements. It should be noted that there is a slight discrepancy in vacuum wavenumbers of spectral features between the current study and that of Cantrell et al.,[18] which is of the order of ∼0.2−0.5 cm^{-1} for different vibronic bands. The vibronic band origins obtained from analysis of data from the current study (see below) agree very well, however, with those reported by Clouthier and Ramsay.[26]

3.3. Spectral Simulations. The spectral simulation program PGOPHER[27] was used to simulate the major vibronic bands of the $\tilde{A}^1A_2-\tilde{X}^1A_1$ electronic absorption spectrum of formaldehyde, using the most comprehensive and recent sets of vibrational-level-dependent rotational constants.[26] The asymmetric top band simulations included all available rotational and centrifugal distortion constants, a thermal Boltzmann distribution of populations over rotational levels of the ground state, and the effects of the statistical weights of nuclear spins of the identical H atoms. As mentioned earlier, each band was simulated at the desired temperature, with inclusion of a Gaussian line width of 0.2 cm^{-1} to mimic the effects of Doppler broadening and the optimum expected laser line width, and inclusion of a further Lorentzian line shape component with fwhm ranging from 0.45−0.7 cm^{-1} depending on the vibronic band (as summarized in Table 2 of the Supporting Information). Figure 6 shows two simulations of the $2^3_0 4^1_0$ vibronic band of HCHO using spectroscopic constants from Clouthier and Ramsay,[26] compared with experimental measurements (top panel). The middle panel of the figure is a simulation of the spectrum that incorporates a Gaussian line width of fwhm 0.07 cm^{-1} (to reproduce the 294 K Doppler broadening of rotational lines). In the bottom panel, the Gaussian width has been increased to 0.2 cm^{-1}, and convolution with a Lorentzian function of line width 0.5 cm^{-1} has been introduced to reproduce correctly the experimentally observed line widths and resolved structure. As explained earlier, power broadening by the UV laser pulse and lifetime broadening by rapid predissociation of the $\tilde{A}$-state levels do not account for the extra line width, which is instead attributed to a 0.35 cm^{-1} fwhm Gaussian UV bandwidth function with an underlying broader component. A noteworthy feature of the central panel of Figure 6 is just how much larger the peak absorption cross sections of HCHO should be if measured with an instrument of resolution equal to, or higher than, the line widths imposed by Doppler broadening.

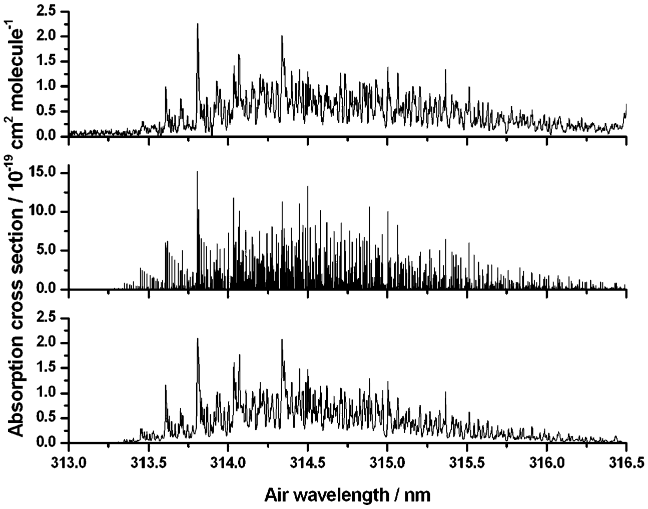

Figure 6. Top: experimental HCHO absorption cross sections for the $2^3_0 4^1_0$ vibronic band. Middle: simulation created using the PGOPHER program with a Gaussian line width of fwhm 0.07 cm^{-1} to mimic the effects of Doppler broadening. Bottom: simulation created using the PGOPHER program with a Gaussian line width of 0.2 cm^{-1} and a Lorentzian line width of 0.5 cm^{-1}.

PGOPHER fitting of the simulation file to the experimental data was employed to refine spectroscopic constants, by matching numerous individual spectral lines in the experimental and simulated spectra and floating various excited-state spectroscopic constants. This fitting procedure had the effect of slightly altering values of the excited-state constants from those reported in the literature. Previously, unrefined simulations of the $2^3_0 4^1_0$ and $2^2_0 4^3_0$ vibronic bands were published,[23] and we present here refined simulations of these bands, and new simulations of all the major vibronic bands between 300 and 340 nm at 294 K in the form of Supporting Information, along with tables of new or refined rotational and centrifugal distortion constants. Figure 7 shows a comparison between experimentally obtained HCHO absorption cross sections for the $2^2_0 4^1_0$ and 2^1_0

TABLE 2: Integrated Band Intensities for the 300−333 nm Region of the $\tilde{A}^1A_2-\tilde{X}^1A_1$ Electronic Absorption of HCHO at Temperatures of 294 and 245 K.

wavenumber interval/ cm^{-1}	vibrational band	294 K-band intensity 10^{-17} cm^2 molecule^{-1} cm^{-1}	245 K-band intensity 10^{-17} cm^2 molecule^{-1} cm^{-1}
32781−33023	$2^4_0 4^1_0$	1.359 ± 0.022	1.379 ± 0.002
32450−32781	$2^3_0 4^3_0$	1.140 ± 0.028	1.055 ± 0.014
32123−32450	$2^1_0 5^1_0$	0.724 ± 0.004	0.753 ± 0.003
31600−31900	$2^3_0 4^1_0$	1.396 ± 0.010	1.442 ± 0.010
31275−31600	$2^2_0 4^3_0$	1.122 ± 0.053	1.099 ± 0.023
30425−30750	$2^2_0 4^1_0$	1.285 ± 0.010	1.310 ± 0.023
30050−30425	$2^1_0 4^3_0$	0.842 ± 0.006	0.823 ± 0.003

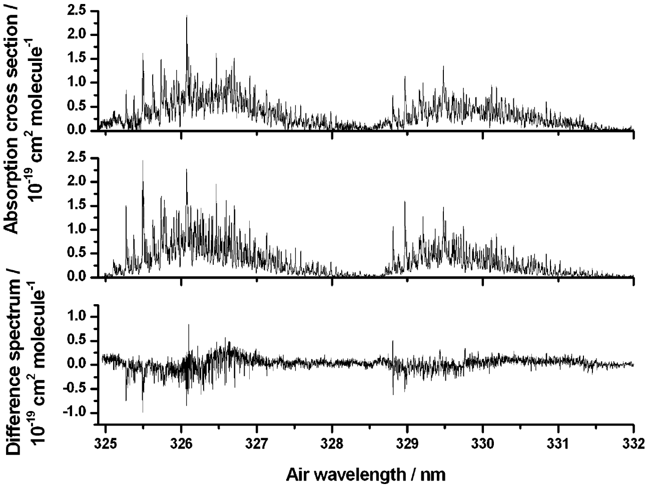

Figure 7. Top: experimental HCHO absorption cross sections for the $2_0^2 4_0^1$ and $2_0^1 4_0^3$ vibronic bands. Middle: simulations created using the PGOPHER program with refined rotational and centrifugal distortion constants at $T = 294$ K. Bottom: difference between the experimental and simulated spectra, plotted on the same vertical scale.

4_0^3 bands and newly simulated spectra. A Lorentzian line width of 0.45 cm^{-1} fwhm was included in the simulation to reproduce correctly the experimentally observed shapes of the spectral lines.

Some underestimation of the intensity of the absorption cross sections, evident toward the high wavelength ends of the bands, may be a consequence of the overlap of other weaker vibronic bands not included in the simulations. Further discrepancies are likely to arise from localized perturbations of $\tilde{A}^1A_2$ state rovibrational energy levels, some of which are mixed with levels of the $\tilde{a}^3A_2$ state. Simulations which use a Gaussian resolution function of fwhm 1.0 cm^{-1} reproduce better the band absorption cross section profiles measured by Cantrell et al.,[18] as a consequence of the reduced resolution, and the resultant loss of some rotational fine structure. Full input simulation files for each vibronic band (at a user-specified resolution) are available in the Supporting Information or from the authors for use with the freely available PGOPHER program.[27] The remaining discrepancies between the simulated and experimental absorption cross sections mean that the simulations should be used with some caution to predict absorption cross sections at temperatures other than those for which experimental values are reported, particularly at high wavelength resolution.

3.4. Effects of N$_2$ Bath Gas. HCHO absorption cross section measurements are of greatest use to atmospheric modelers, and for spectroscopic retrieval of HCHO mixing ratios, when the effects of ambient gas pressure have been quantified. Measurements were thus undertaken of the $\tilde{A}^1A_2-\tilde{X}^1A_1$ rovibronic absorption spectrum of HCHO with the addition of different pressures of nitrogen bath gas. Pressure-broadening is well-known to reduce peak absorption cross sections of narrow spectral lines and cause nearby lines to merge. A small but highly structured wavelength region was chosen and the effects of different pressures of nitrogen bath gas were determined for the same partial pressure of HCHO. The HCHO absorption cross sections for the whole wavelength range, 300−340 nm, were then measured with an added pressure of 200 Torr of N$_2$ bath gas (data are available as Supporting Information). Figure 8 shows the effects of 200 and 500 Torr of N$_2$ bath gas on the HCHO absorption cross sections for a small region of the $2_0^1 4_0^1$ band. There is little discernible change in the overall magnitudes at the peaks of absorption, but a modest degree of pressure broadening (and loss of resolution) is evident in the line shapes. This broadening was estimated to correspond to ~0.2−0.3 cm^{-1} atm^{-1} for N$_2$. There are no isolated lines for excitation to a single rovibrational quantum state that can be fitted to Voigt line shape functions for more precise quantification of pressure broadening coefficients. These coefficients are thus estimated by eye from comparison of experimental data and spectral simulations, as demonstrated by Figure 9; the top panel shows experimental HCHO absorption cross sections for the $2_0^2 4_0^1$ vibronic band measured at 294 K with the addition of 500 Torr of nitrogen bath gas, and the bottom panel is a simulation created using the PGOPHER program, with an additional 0.15 cm^{-1} included in the Lorentzian line width to account for pressure broadening.

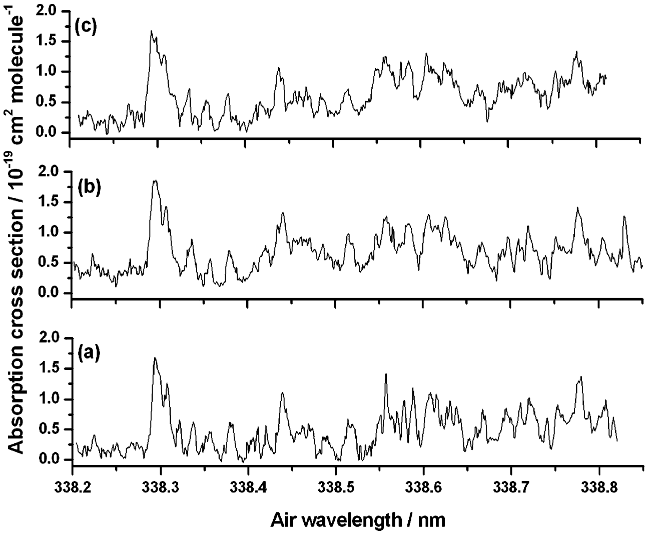

Figure 8. Absorption cross sections of HCHO for a small region of the $2_0^1 4_0^1$ band of the $\tilde{A}^1A_2-\tilde{X}^1A_1$ transition, showing the effects of different pressures of nitrogen bath gas: (a) 0 Torr; (b) 200 Torr; (c) 500 Torr.

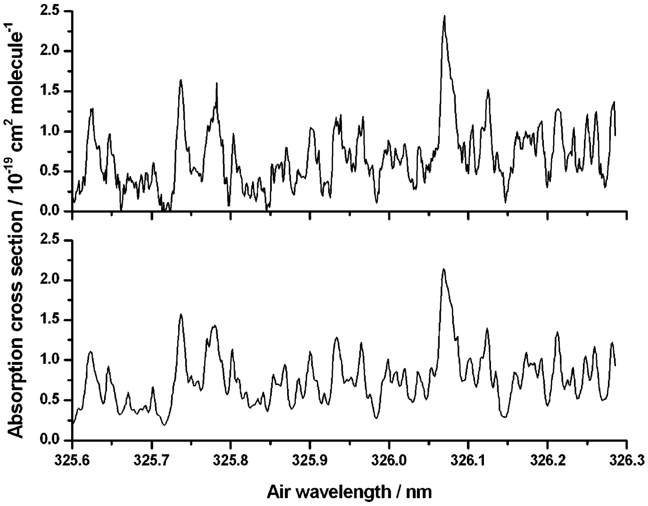

Figure 9. Top panel: experimental HCHO absorption cross sections for the $2_0^2 4_0^1$ vibronic band at 294 K with the addition of 500 Torr nitrogen bath gas. Bottom: simulation created using the PGOPHER program with refined spectroscopic constants from the current work, and an additional 0.15 cm^{-1} added to the Lorentzian line width to account for the effects of pressure broadening.

3.5. Temperature Dependence of the Spectra. The decrease of temperature with altitude in the troposphere necessitates knowledge of HCHO absorption cross sections at varying temperatures, both to understand the impact on HCHO photo-

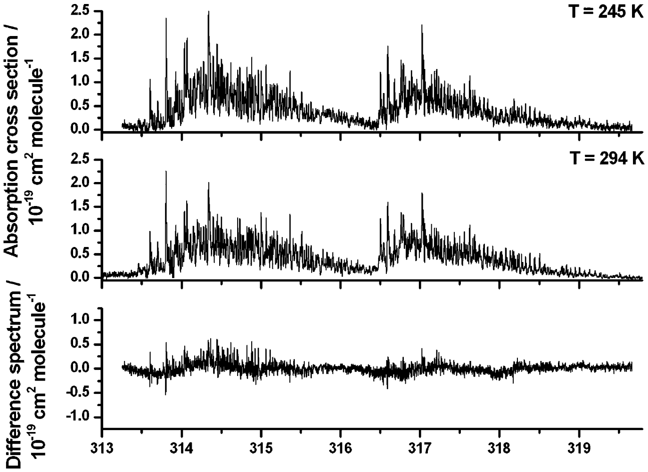

Figure 10. Absorption cross sections of the HCHO $\tilde{A}^1A_2-\tilde{X}^1A_1$ $2^3_0 4^1_0$ and $2^2_0 4^3_0$ bands recorded at the temperatures 294 K (middle panel) and 245 K (top panel). The difference spectrum (bottom panel) is obtained by subtraction of the 294 K data from the 245 K data.

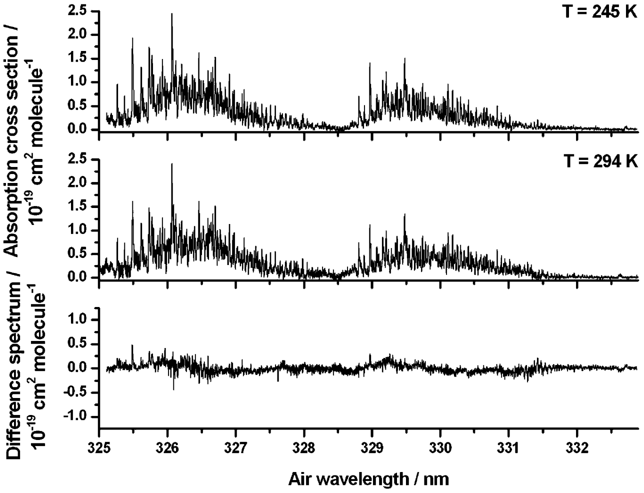

Figure 11. Absorption cross sections of the HCHO $\tilde{A}^1A_2-\tilde{X}^1A_1$ $2^2_0 4^1_0$ and $2^1_0 4^3_0$ bands recorded at the temperatures 294 K (middle panel) and 245 K (top panel), together with the difference spectrum (bottom panel) obtained by subtraction of the 294 K data from the 245 K data.

chemistry and for altitude-dependent retrievals of mixing ratios by UV spectroscopy. As a first step toward determining HCHO absorption cross sections at temperatures in the range expected for the troposphere (down to ∼208 K), the internal temperature of the vacuum chamber was reduced to 245 K and spectroscopic data were recorded at this temperature in the wavelength range 300−340 nm. The temperature dependence could, in principle, be determined from the spectral simulations described earlier; for unperturbed bands, high quality simulations require knowledge of precise rotational constants for the ground and excited vibronic states, and calibration of the absolute peak intensities at one temperature. As was, however, evident from the intercomparison of experimental spectra and simulations, underlying vibronic bands and any perturbations of rotational energy levels must also be characterized for fully quantitative simulations (unless working at much-reduced wavelength resolution). The experimental data at lower temperature are an additional check of the reliability of the simulations prior to their use for calculation of absorption cross sections for any other required tropospheric temperature. Figures 10 and 11 show absorption cross sections of the HCHO $\tilde{A}^1A_2-\tilde{X}^1A_1$ $2^3_0 4^1_0$, $2^2_0 4^3_0$, $2^2_0 4^1_0$, and $2^1_0 4^3_0$ bands, covering the wavelength region 313−333 nm, recorded at temperatures of 294 K (middle panel) and 245 K (top panel). Comparison of the two data sets, along with the difference spectrum ($\sigma_{245K} - \sigma_{294K}$, bottom panel), shows that at the maximum of each absorption band, the temperature effects are strongest, with lower temperatures giving greater peak intensities. At the long wavelength side of each band, the temperature effect is reversed and lower temperatures result in smaller absorption cross sections. With a reduction in temperature, the intensities of rotational lines are observed to increase for lines originating from low to mid J'' rotational levels (up to $J'' \sim 11$), and to decrease for high J'' levels (18 and above), as expected for a Boltzmann distribution of populations. A similar effect was seen by comparing simulations of each vibronic band at the two experimental temperatures, as shown in Figure 12 in the case of the $2^2_0 4^1_0$ band.

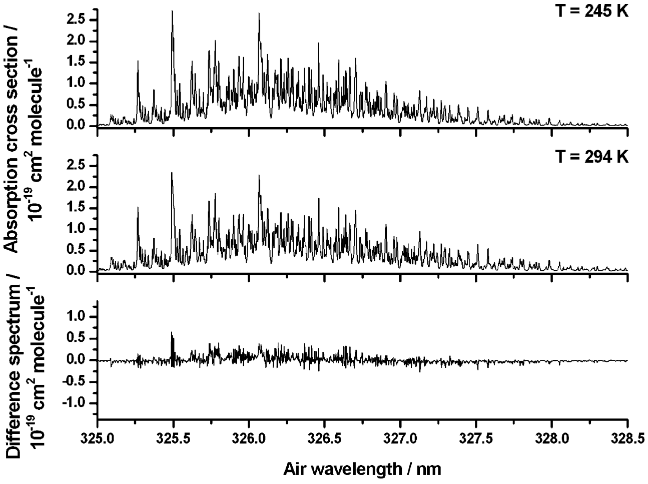

Figure 12. Simulated absorption cross sections of the HCHO $\tilde{A}^1A_2-\tilde{X}^1A_1$ $2^2_0 4^1_0$ bands at 294 K (middle panel) and 245 K (top panel), together with a difference spectrum (bottom panel) obtained by subtraction of the 294 K data from the 245 K data.

Using the vibrational frequencies for HCHO in the $\tilde{X}^1A_1$ state,[26] the vibrational partition functions and thus the fraction of all HCHO molecules occupying the $v'' = 0$ vibrational level were calculated for the two experimental temperatures. The calculated percentage difference between the two partition functions was found to be negligible, indicating that vibrational band-integrated absorption cross sections should not change over the 245−294 K temperature range. If the temperature is further reduced to 220 K, the calculated percentage difference in the integrated band intensities is still found to be only ∼1%. Table 2 shows experimental band-integrated absorption cross sections obtained at 245 K compared to those at 294 K.

4. Conclusions

We present high resolution formaldehyde absorption cross sections for all the major vibronic bands in the $\tilde{A}^1A_2-\tilde{X}^1A_1$ electronic absorption spectrum between 300 and 340 nm under varying pressure and temperature conditions. The absorption cross sections are measured at an estimated Gaussian resolution of 0.0035 nm (0.35 cm^{-1}) fwhm, which improves on previously published data (1 cm^{-1} resolution by Cantrell et al.,[18] 2.73 cm^{-1} by Meller and Moortgat[20]). The peak absorption cross sections of lines of highly structured bands of HCHO will still be underestimated unless the resolution of the spectrometer is comparable to, or narrower than, the natural widths of the sharpest spectral features. Spectral simulations can, however, be used to predict peak absorption cross sections at resolutions as high as the line widths imposed by Doppler and pressure broadening. Wavelength-dependent absorption cross sections obtained under the various experimental conditions described, as well as values obtained by convolution with 0.1, 0.2 and 1.0 nm fwhm Gaussian functions, are available as Supporting Information. Figures of 294 K spectral simulations of wavelength-dependent absorption cross sections for all the major vibronic bands are also included as Supporting Information, along with the refined rotational and centrifugal distortion constants used in the simulations. The input files for the spectral simulation program PGOPHER[27] are available from the authors and can be used to generate simulated spectra for individual vibronic bands at a user-specified temperature and spectral resolution.

Acknowledgment. Funding for equipment and for FDP from the NERC *Upper Troposphere and Lower Stratosphere* programme, and from EPSRC for studentships for CAS and BC is gratefully acknowledged. We thank K. N. Rosser for considerable technical assistance, Prof. M. N. R. Ashfold, Dr. D. E. Shallcross, Dr. H.-P. Loock, and Dr. A. L. Holloway for valuable discussions, Dr. C. M. Western for advice and help with fitting and simulation of spectra using PGOPHER, and Dr. C. A. Cantrell and Prof. G. K. Moortgat for provision of their spectroscopic data. A.J.O.E. gratefully acknowledges the award of a Senior Research Fellowship by the Leverhulme Trust.

Supporting Information Available: Tabulated numerical data for HCHO absorption cross sections for the $\tilde{A}^1A_2-\tilde{X}^1A_1$-electronic absorption spectrum between the wavelengths 300 and 340 nm at two temperatures, 294 and 245 K; HCHO absorption cross sections measured with the addition of 200 Torr of nitrogen bath gas at 294 K for the major vibronic bands in the $\tilde{A}^1A_2-\tilde{X}^1A_1$ electronic absorption spectrum; figures of spectral simulations of the major vibronic bands of the HCHO $\tilde{A}^1A_2-\tilde{X}^1A_1$ electronic absorption spectrum and tables of the refined spectroscopic parameters; and spectral simulation files for use with PGOPHER to simulate HCHO absorption cross sections at any desired resolution and temperature. This material is available free of charge via the Internet at http://pubs.acs.org.

References and Notes

(1) Wuebbles, D. J.; Hayhoe, K. *Earth Sci. Rev.* **2002**, *57*, 177−210.

(2) Sprengnether, M.; Demerjian, K. L.; Donahue, N. M.; Anderson, J. G. *J. Geophys. Res.* **2002**, *107*, 4268−4281.

(3) Riedel, K.; Weller, R.; Schrems, O. *Phys. Chem. Chem. Phys.* **1999**, *1*, 5523−5528.

(4) Williams, I. D.; Revitt, D. M.; Hamilton, R. S. *Sci. Total Environ.* **1996**, *189/190*, 475−483.

(5) Grosjean, D.; Swanson, R. D. *Sci. Total Environ.* **1983**, *29*, 65−85.

(6) DeMore, W. B.; Sander, S. P.; Golden, D. M.; Hampson, R. F.; Kurylo, M. J.; Howard, C. J.; Ravishankara, A. R.; Kolb, C. E.; Molina, M. J. *Data for use in stratospheric modelling*; Evaluation No. 12, JPL Publ. 97-4; Jet Propulsion Laboratory: Pasadena, CA, 1997.

(7) Wennberg, P. O.; Hanisco, T. F.; Jaegle, L.; Jacob, D. J.; Hinsta, E. J.; Lanzendorf, E. J.; Anderson, J. G.; Gao, R. S.; Keim, E. R.; Donnelly, S. G.; Del Negro, L. A.; Fahey, D. W.; McKenn, S. A.; Salawitch, R. J.; Webster, C. R.; May, R. D.; Herman, R. L.; Proffitt, M. H.; Marigtan, J. J.; Atlas, E. L.; Schauffler, S. M.; Flocke, F.; McElroy, C. T.; Bui, T. P. *Science* **1998**, *279*, 49−53.

(8) Jaeglé, L.; Jacob, D. J.; Wennberg, P. O.; Spivakovsky, C. M.; Hanisco, T. F.; Lanzendorf, E. J.; Hintsa, E. J.; Fahey, D. W.; Keim, E. R.; Proffitt, M. H.; Atlas, E. L.; Flocke, F.; Schauffler, S.; McElroy, L. T.; Midwinter, C.; Pfister, L.; Wilson, J. C. *Geophys. Res. Lett.* **1997**, *24*, 3181−3184.

(9) Müller, J.-F.; Brasseur, G. *J. Geophys. Res.* **1999**, *104*, 1705−1715.

(10) Valachovic, L. R.; Tuchler, M. F.; Dulligan, M.; Droz-Georget, T.; Zyrianov, M.; Kolessov, A.; Reisler, H.; Wittig, C. *J. Chem. Phys.* **2000**, *112*, 2752−2761.

(11) Hausmann, M.; Brandenburger, U.; Brauers, T.; Dorn, H.-P. *J. Geophys. Res.* **1997**, *102*, 16011−16022.

(12) Luo, M.; Beer, R.; Jacob, D. J.; Logan, J. A.; Rogers, C. D. *J. Geophys. Res.* **2002**, *107*, 4270−4280.

(13) Grossman, D.; Moortgat, G. K.; Kibler, M.; Schlomski, S.; Bachmann, K.; Alicke, B.; Geyer, A.; Platt, U.; Hammer, M. U.; Vogel, B.; Mihelcic, D.; Hofzumahaus, A.; Holland, F.; Volz-Thomas, A. *J. Geophys. Res.* **2003**, *108*, 8250−8270.

(14) Sinreich, R.; Friess, U.; Wagner, T.; Platt, U. *Faraday Discuss.* **2005**, *130*, 153−164.

(15) Dieke, G. H.; Kistiakowsky, G. B. *Phys. Rev.* **1934**, *45*, 4−28.

(16) McQuigg, R. D.; Calvert, J. G. *J. Am. Chem. Soc.* **1969**, *91*, 1590−1599.

(17) Bass, A. M.; Glasgow, L. C.; Miller, C.; Jenson, J. P.; Filkin, D. L. *Planet. Space Sci.* **1980**, *28*, 675−679.

(18) Cantrell, C. A.; Davidson, J. A.; McDaniel, A. H.; Shetter, R. E.; Calvert, J. G. *J. Phys. Chem.* **1990**, *94*, 3902−3908.

(19) Rogers, J. D. *J. Phys. Chem.* **1990**, *94*, 4011−4015.

(20) Meller, R.; Moortgat, G. K. *J. Geophys. Res.* **2000**, *105*, 7089−7101.

(21) Co, D. T.; Hanisco, T. F.; Anderson, J. G.; Keutsch, F. N. *J. Phys. Chem. A* **2005**, *109*, 10675−10682.

(22) Pope, F. D.; Smith, C. A.; Davis, P. R.; Shallcross, D. E.; Ashfold, M. N. R.; Orr-Ewing, A. J. *Faraday Discuss.* **2005**, *130*, 59−73.

(23) Pope, F. D.; Smith, C. A.; Ashfold, M. N. R.; Orr-Ewing, A. J. *Phys. Chem. Chem. Phys.* **2005**, *7*, 79−84.

(24) Spence, R.; Wild, W. J. *J. Chem. Soc.* **1935**, *1*, 338−340.

(25) Moore, C. B.; Weisshaar, J. C. *Ann. Rev. Phys. Chem.* **1983**, *34*, 525−555.

(26)) Clouthier, D. J.; Ramsay, D. A. *Annu. Rev. Phys. Chem.* **1983**, *34*, 31−58.

(27)) Western, C. M. PGOPHER, a Program for Simulating Rotational Structure, University of Bristol, 2005, http://pgopher.chm.bris.ac.uk.